ISSS Journal of Micro and Smart Systems (2020) 9:55–68
https://doi.org/10.1007/s41683-020-00048-z

ORIGINAL ARTICLE

Effect of flapping orientation on caudal fin propelled bio-inspired underwater robots

Santhosh Ravichandran[1] · Srikanth Dharwada[1] · Aman Agarwal[1] · Prabhu Rajagopal[1]

Received: 3 November 2019 / Revised: 15 December 2019 / Accepted: 28 January 2020 / Published online: 24 February 2020

Abstract

Aquatic animals and mammals in nature, in particular, the Body and/or Caudal Fin (BCF) swimmers swim either by flapping their fins in the sideways direction or the dorso-ventral direction. Not much literature is available on the effects of the performance of these robots based on the choice of its flapping orientation. In this research, it is found that dorso-ventral flapping could lead to better self-stabilizing effects and lesser energy consumption compared to sideways flapping. It is also found that the choice of dorso-ventral flapping offers the possibility of controlling the body's oscillation amplitude while flapping. This is an appealing advantage for underwater surveying robots carrying cameras and sensors as controlled body oscillations could yield better results from its payloads. The main body of results is obtained with simulations for underwater vehicle dynamics with the coefficients of the REMUS underwater vehicle, while stability analysis for a generalised case is also presented.

Keywords Bio-inspired underwater robotics · Caudal fin flapping orientation · Underwater vehicle dynamics

Introduction

Remotely operated and automated robotic submersibles are today widely used for applications such as inspection, intervention and exploration. As with other fields, there is a growing interest in bio-inspired and bio-mimetic concepts for various elements of submersibles, including propulsion. Bio-inspired propulsion has advantages including efficiency, ability to navigate in complex environments, and is particularly attractive for applications needing stealth. For example, studies of ecological habitats of marine organisms and naval expeditions would benefit from minimally intrusive bio-inspired propulsion. Set in this context, this paper explores the relationship of the flapping orientation of bio-inspired fin-like propulsion systems on the swimming performance of small underwater submersibles, a topic not widely studied in the literature. This research supplements recently published work from the authors' research group on the mechanics of bioinspired caudal fin propulsion for small remotely operated vehicles (Krishnadas et al. 2018).

Cetaceans, sirenians, phocids and other marine mammals have adopted dorso-ventral oscillations of their caudal propulsors for propulsion. On the other hand, fishes and some swimming reptiles use sideways oscillations of their caudal propulsors or body undulations for propulsion. The reason for such a difference in flapping orientation in nature is perhaps because of the secondary evolution of aquatic mammals while moving from land to water. Initially, terrestrial mammals evolved to realign their limbs from a primitive tetrapod configuration for efficient cursorial movement on land (Jimenez et al. 2010). Some species of such mammals, while moving to water, evolved towards lift-based propulsion for efficient swimming by going through phases of paddling gaits with their quadruped limbs that eventually evolved to dorso-ventral flapping of caudal flukes (Xia et al. 2016). Therefore, there does not seem to be any evidence of performance-driven reasons for different flapping orientations in marine species, which is rather attributed to their differing evolutionary paths.

✉ Santhosh Ravichandran
santhosh11dec@gmail.com

[1] Centre for Nondestructive Evaluation, Department of Mechanical Engineering, Indian Institute of Technology (IIT) Madras, Chennai, Tamil Nadu 600036, India

Aspects of stability and manoeuvrability have been studied extensively in the context of marine vehicles and also to some extent in fishes and mammals (Lewis 1989; Fish 2004). In general, fishes and aquatic mammals have their center of mass above the center of buoyancy due to the distribution of heavier tissues on the dorsal side (or the ventral position of swim bladder in some species (Fish 2004). Although this is intrinsically unstable, fishes counteract this instability by producing corrective forces with their fins. However, in man-made systems, it is desirable to have a positive metacentric height (Fish 2016) i.e., the center of mass positioned below the center of buoyancy to avoid complexity in control and to reduce power consumption (Liu 2016). In doing so, for biomimetic caudal fin propelled underwater vehicles, the dynamics of such a mass distribution would be different for dorso-ventral and sideways flapping. A positive metacentric height for the vehicle yields stiffness in the pitching axis which could interact with the moments from dorso-ventral flapping. This is not the case in sideways flapping as the forces and moments are not aligned with the pitching axis. The effects of this principle are discussed in detail in this paper. We identify that the choice of flapping orientation for a biomimetic vehicle could have an impact on its energetics, stability and propulsive performance.

The energetics of caudal fin propelled swimmers could be related to their Center of Mass (COM) oscillations (Lauder and Drucker 2002; Lauder 2000). Similar to terrestrial locomotion, caudal fin propelled swimmers with large COM oscillation amplitudes may have a higher cost of transport leading to lower efficiencies (Lauder and Drucker 2002). Therefore, the ability to reduce COM oscillation amplitudes by design could be beneficial. We find that the choice of dorso-ventral flapping could help in this aspect and that the choice of sideways flapping would always require an active control system intervention to achieve an equivalent performance. In this article, we analyse and discuss this topic based on the distance travelled by the swimmer for the same thrust input and duration.

The ability to control the body's oscillatory (rotational) amplitude along the flapping axis could be useful in improving the hydrodynamic propulsive performance (Lauder 2015a, b; Xiong and Lauder 2014) and also in reducing disturbances for on-board sensor measurements. The parallel alignment of the restoring and flapping torque axes in dorso-ventral flapping means that the flapping frequency or the metacentric height can be adjusted to optimise the body rotational oscillation amplitudes. On the contrary, for sideways flapping, such control over rotational amplitudes would not be possible without changing the shape of the body, which in turn might lead to changing mass distribution or negative hydrodynamic effects. Motivated by the potential advantages, a qualitative relation between flapping frequency, rotational amplitude and metacentric height is given for a few cases.

Here, we investigate the effects of the choice of flapping orientation using underwater dynamics simulations with the body dynamic model of an autonomous underwater vehicle (AUV) (for more details, please see "Methods"). In our numerical model, the conventional rotary thruster is replaced with a bio-inspired flapping propulsor. Hence, the analysis is limited to thunniform swimming modes for simplicity. Nevertheless, this paper will serve to highlight the potential advantages or effects of the choice of flapping orientation on the swimming performance, (stability analysis for a generalised case is also reported in "Appendix B"). As per our survey of literature, such a study is being reported for the first time.

The paper is organised as follows. Firstly, the methods section below provides information on the procedure for numerical simulations and analysis. Next, the results section presents the effects of flapping orientation on stability, COM oscillations and rotational oscillation amplitude. Finally, the paper concludes after a discussion of the results.

Methods

6-DOF mathematical model

To simulate the motion of the swimmer in three-dimensional space, the system is solved for the body-fixed frame and transformed to the inertial or earth fixed frame. A set of six equations—three to model the linear movements and the rest for rotational movements, govern the dynamics of the system. The kinematic and dynamic model of the system in consideration is similar to the model used (Goldberg 1988). Society of Naval Architects and Marine Engineers (SNAME) (Morrison 1987) convention is followed throughout this article. In Eq. (1a, 1b, 1c, 1d), vector η represent position (η_1) and orientation (η_2) in the inertial frame; vector v represents the translational and rotational velocities in the body-fixed frame. Throughout the article, $x, y, z, \emptyset, \theta, \psi$ represent surge, sway, heave, roll, pitch and yaw, respectively, and u, v, w, p, q, r represent their velocities. The origin of the body-fixed frame is taken to be at the center of buoyancy.

$$\eta = [x, y, z, \emptyset, \theta, \psi]^T \tag{1a}$$

$$\eta_1 = [x, y, z]^T \tag{1b}$$

$$\eta_2 = [\phi, \theta, \psi]^T \tag{1c}$$

$$v = [u, v, w, p, q, r]^T \tag{1d}$$

The matrices $J_1(\eta_2)$ and $J_2(\eta_2)$ in Eq. (2) transform linear and angular velocities from a body-fixed coordinate system to the inertial frame coordinate system.

$$[\dot{x},\dot{y},\dot{z}]^T = J_1(\eta_1)[u,v,w]^T; \quad \left[\dot{\phi},\dot{\theta},\dot{\psi}\right]^T = J_2(\eta_2)[p,q,r]^T \tag{2}$$

where

$$J_1(\eta_1) = \begin{bmatrix} c(\psi)c(\theta) & -s(\psi)c(\emptyset) + c(\psi)s(\theta)s(\emptyset) & s(\psi)s(\emptyset) + c(\psi)c(\emptyset)s(\theta) \\ s(\psi)c(\theta) & c(\psi)c(\emptyset) + s(\emptyset)s(\theta)s(\psi) & -c(\psi)s(\emptyset) + s(\theta)s(\psi)c(\emptyset) \\ -s(\theta) & c(\theta)s(\emptyset) & c(\theta)c(\emptyset) \end{bmatrix} \tag{3}$$

$$J_2(\eta_2) = \begin{bmatrix} 1 & s(\emptyset)t(\theta) & c(\emptyset)t(\theta) \\ 0 & c(\psi)c(\emptyset) + s(\emptyset)s(\theta)s(\psi) & -s(\emptyset) \\ 0 & s(\emptyset)/c(\theta) & c(\emptyset)/c(\theta) \end{bmatrix} \tag{4}$$

In Eqs. (3) and (4) and in the rest of this document, the symbols c, s and t correspond to cos, sin and tan operators, respectively. The following expression defines the rigid body dynamics in 6-degrees of freedom system with respect to the body-fixed frame. X, Y and Z represent forces in the surge, sway and heave axes, whereas K, M and N represent moments along roll, pitch and yaw axes.

$$M_A\dot{v} = [X,Y,Z,K,M,N]^T + \tau^T \tag{5}$$

where

$$\begin{aligned} X = {} & -(W-B)\sin(\theta) + X_{uu}u|u| + (X_{wq}-m)wq + \left(X_{qq}+mx_g\right)q^2 \\ & + (X_{vr}+m)vr + \left(X_{rr}+mx_g\right)r^2 - my_gpq - mz_gpr \end{aligned} \tag{6}$$

$$\begin{aligned} Y = {} & (W-B)\cos(\theta)\sin(\emptyset) + Y_{vv}v|v| + Y_{rr}r|r| + Y_{uv}uv \\ & + \left(Y_{wp}+m\right)wp + (Y_{ur}-m)ur - mz_gqr + \left(Y_{pq}-mx_g\right)pq \\ & + Y_{uu\delta_r}u^2\delta_r \end{aligned} \tag{7}$$

$$\begin{aligned} Z = {} & (W-B)\cos(\theta)\cos(\emptyset) + Z_{ww}w|w| + Z_{qq}q|q| + Z_{uw}uw \\ & + \left(Z_{uq}+m\right)uq + \left(Z_{vp}-m\right)vp + \left(mz_g\right)p^2 + \left(mz_g\right)q^2 \\ & + \left(Z_{rp}-mx_g\right)rp \end{aligned} \tag{8}$$

$$\begin{aligned} K = {} & K_{pp}p|p| - \left(y_gW - y_bB\right)\cos(\theta)\cos(\emptyset) \\ & - \left(z_gW - z_bB\right)\cos(\theta)\sin(\emptyset) \\ & - \left(I_{zz}-I_{yy}\right)rp + mz_gwp + mz_gur \end{aligned} \tag{9}$$

$$\begin{aligned} M = {} & -\left(z_gW - z_bB\right)\sin(\theta) - \left(x_gW - x_bB\right)\cos(\theta)\cos(\emptyset) \\ & + M_{ww}w|w| + M_{qq}q|q| + \left(M_{rp} - (I_{xx}-I_{zz})\right)rp \\ & + mz_gvr - mz_gwq + \left(M_{uq} - mx_g\right)uq \\ & + M_{uw}uw + (M_{vp} + mx_g)vp \end{aligned} \tag{10}$$

$$\begin{aligned} N = {} & -\left(x_gW - x_bB\right)\cos(\theta)\sin(\emptyset) - \left(y_gW - y_bB\right)\sin(\theta) \\ & + N_{vv}v|v| + N_{rr}r|r| + N_{uv}uv \\ & + \left(N_{pq} - \left(I_{yy}-I_{xx}\right)\right)pq + \left(N_{wp} - mx_g\right)wp \\ & + \left(N_{ur} + mx_g\right)ur + N_{uu\delta_r}u^2\delta_r \end{aligned} \tag{11}$$

$$\begin{aligned} \tau = {} & \left[\left|X_{\text{prop}}\sin(2\pi t)\right|, Y_{\text{prop}}\sin(2\pi t)\right. \\ & \left. + Y_{\text{dist}}, Z_{\text{prop}}\sin(2\pi t), K_{\text{prop}}, M_{\text{prop}}\sin(2\pi t), N_{\text{prop}}\sin(2\pi t)\right] \end{aligned} \tag{12}$$

$$M_A = \begin{bmatrix} m - X_{\dot{u}} & 0 & 0 & 0 & mz_g & -my_g \\ 0 & m - Y_{\dot{v}} & 0 & -mz_g & 0 & mx_g - Y_{\dot{r}} \\ 0 & 0 & m - Z_{\dot{w}} & my_g & -Z_{\dot{q}} & 0 \\ 0 & -mz_g & my_g & I_{xx} - K_{\dot{p}} & 0 & 0 \\ mz_g & 0 & -mx_g - M_{\dot{w}} & 0 & I_{yy} - M_{\dot{q}} & 0 \\ -my_g & mx_g - N_{\dot{v}} & 0 & 0 & 0 & I_{zz} - N_r \end{bmatrix} \tag{13}$$

Equation (5) is solved for $\dot{v}$ along with Eq. (2) for v and then for η with the 'ode15s' function of MATLAB (Cook 2012).

M_A in the LHS of Eq. (5) consists of the inertia and added mass terms. The first term in the RHS consists of contributions from cross-flow, centrifugal, coriolis, fin lift, hydrostatic and drag terms, whereas the second term of the RHS consists of forces acting on the body including propulsion forces and external perturbations. Dorso-ventral flapping is modelled by assigning zero to Y_{prop} and N_{prop} in Eq. (12) and sideways flapping is modelled without Z_{prop} and M_{prop}. The fin lift terms are included only in the sway and yaw equations (Eqs. 8 and 11) as only rudder control was simulated in this study (to correct the vehicle to swim in a straight line in sideways flapping cases). In addition, the propulsive forces assumed to be sinusoidal in nature, based on the results from Li et al. ("MATLAB 2014a) where thrust and lateral forces are shown to be nearly sinusoidal. The values of these forces, along with other parameters and non-linear coefficients are listed in Table 1.

Results

Numerical 6 degrees of freedom (DOF) simulations for underwater vehicle dynamics were performed with the body dynamic coefficients of REMUS underwater vehicle (Goldberg 1988). REMUS is symmetric about two planes (XZ and XY, see Fig. 1) with similar body dynamic parameters for both flapping orientations, therefore, allowing a fair comparison. The directions of dorso-ventral and sideways flapping axes are indicated in Fig. 1.

Stability of the test model

To test the self-stability (stability without active control inputs) of the vehicle against external disturbances such as ocean currents and collisions, a force of 10 N was applied in the sway direction (positive Y, see Fig. 1) while the vehicle is swimming forward for a short time period. Studies of disturbances in the heave direction yielded similar results for both flapping orientations. Simulation results of the path of the vehicle with different axes of flapping under these conditions are presented in Fig. 2. Interestingly, with sideways flapping, even without any external disturbances, the swimmer seems to tend to a circular path. However, under the same conditions, the swimmer with dorso-ventral flapping behaves as expected, taking a straight-line path without a disturbing force and a circular path with disturbance. It is also interesting to note that, in all these cases, once the vehicle starts tracing a circular path, it continues to do so indefinitely. This behaviour is explained in Fig. 3.

The cause for motion in a circular path is the sway/yaw coupling of the body. A positive velocity in the sway direction ($+ v$) along with a positive forward velocity ($+ u$) causes the vehicle to turn in negative direction of the yaw axis. This is because of the cross-flow term which, in this case, is more dominated by the characteristics of the body than the rudder. On the other hand, acceleration in the sway direction will cause the body to turn in the positive direction of yaw axis because of the added mass term being dominant from the rear portion of the body and rudder fins. This said the physics of such circling behaviour can be explained by breaking down the sequence of events:

(1) While the swimmer is moving with a forward velocity, a force of 10 N was applied on the origin of the body coordinate frame for 1 s in the $+ Y$ direction (see Fig. 3a).
(2) This force causes the vehicle to accelerate in the $+ Y$ direction with velocity, v. This acceleration in turn causes the vehicle to turn in the positive yaw

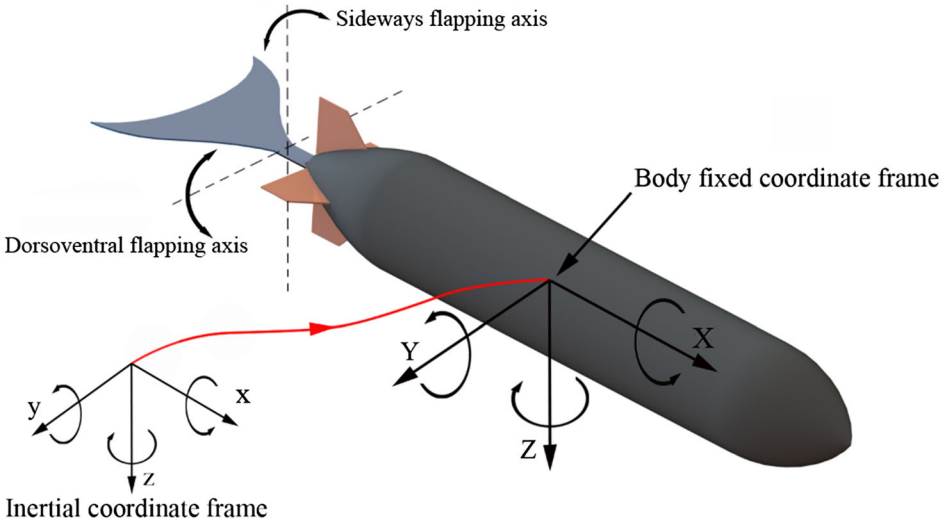

Fig. 1 The model used for numerical analysis. Illustration of the model considered for simulations along with its coordinate frames indicating positive directions of linear and rotational axes. The model shown here represents dorso-ventral flapping

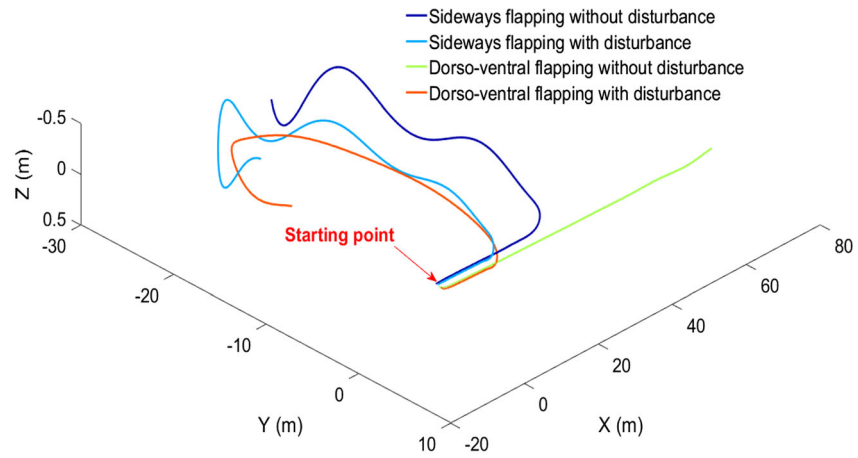

(a) Isometric view

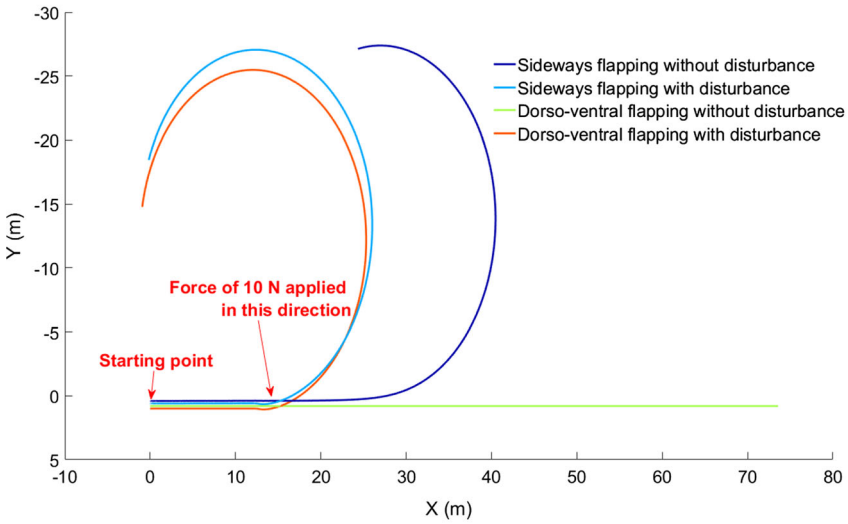

(b) Top view

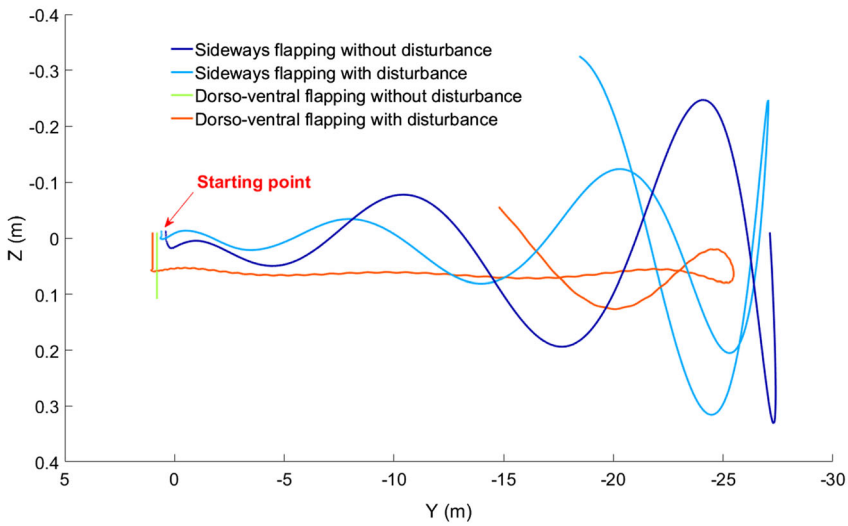

(c) Front view

Fig. 2 Simulated paths of the two different flapping orientations. Simulated path of the AUV to compare the stability of dorso-ventral flapping and sideways flapping with and without disturbance. A disturbing force of 10 N was applied for 1 s after 36 s of forward swimming (in $+X$ direction) which is at about $X \sim 10$ m in these plots. **a**–**c** Shows the path of the AUV in isometric, top and front views, respectively

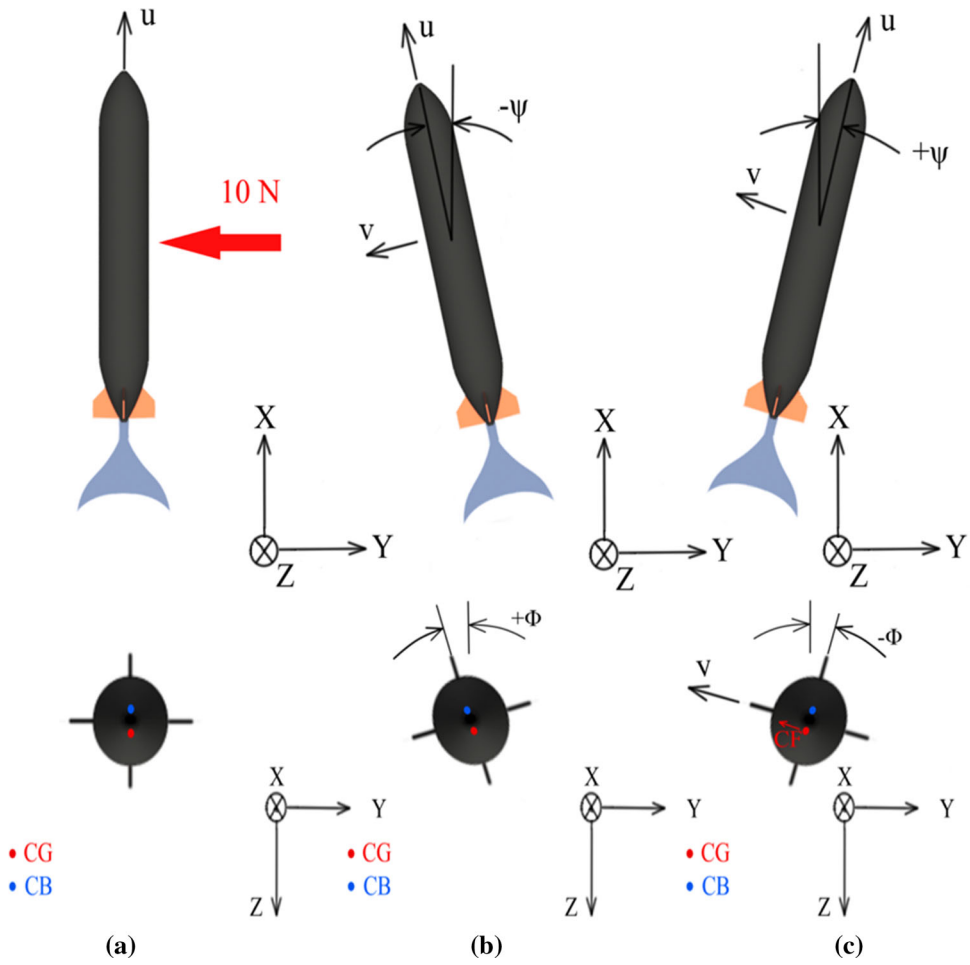

Fig. 3 Schematics to explain instability. Illustration of numerical results through top view and front view of the body while undergoing a swaying force of 10 N. CG represents center of gravity and CB represents center of buoyancy. Center of buoyancy is also the origin of body co-ordinate system. **a** The body is moving in a straight line just before the application of sideways disturbance force, **b** body accelerating in + *Y* direction after application of disturbance of 10 N for 1 s, **c** body changing its direction of yaw due to the effect of the disturbance

direction due to the aforementioned crossflow term (see Fig. 3b). This rotation attenuates with low accelerations. Also, since the location of the force application is above the center of gravity (CG), the body rolls slightly in the positive direction (see Fig. 3b). In the case of a swimmer with sideways flapping, an initial drift in the direction of the *Y* axis due to initial flapping gives a non-zero value of velocity, *v* in the *Y* direction.

(3) After the period of acceleration, cross-flow terms begin to dominate. As the velocity *v* grows, the body is rotated in the negative direction of yaw due to the cross-flow torque. This is illustrated in Fig. 3c.

(4) A rotation in the yaw axis while moving forward yields a curved path. The body also rolls to a negative roll angle due to torque from the centrifugal force on the center of gravity (see Fig. 3c) from the resulting curved path.

(5) However, continuation in such a curved path needs a constant torque in the yaw direction. This is given by the generation of sway velocity, *v* due to the centrifugal force. A non-zero sway velocity along with a forward velocity again leads to a negative yawing torque with influence from cross-flow terms as said in step (3) and the vehicle continues a curved path.

(6) Steps (3)–(5) are repeated indefinitely and the swimmer continues this circular path.

A similar type of motion is known in aircrafts as the spiral mode (Li et al. 2017), in which an aircraft would spiral dive towards the ground if a disturbing force is applied. The longitudinal oscillation observed in Fig. 2 is also because of the cross-flow terms resulting from velocities in the surge and heave directions (*X* and *Z*, respectively) similar to the phugoid mode (Li et al. 2017) in aircrafts. However, in this case, a restoring torque due to longitudinal stability (from positive metacentric height) of the vehicle limits this value from growing indefinitely. Figure 4 shows the paths for a vehicle with dorso-ventral flapping of different values of metacentric height (z_g) and a disturbing force applied in the sway direction. Also, as the metacentric height tends to zero (blue line in Fig. 4) the COM oscillations amplify. This trend is due to the lack of sufficient restoring moment (with decreasing metacentric height) for the swimmer to control the pitching moment

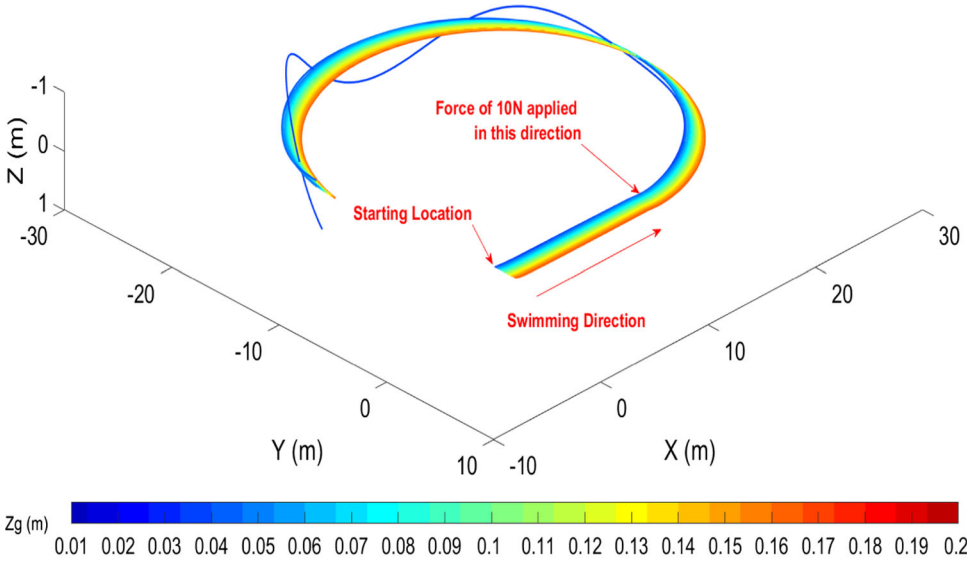

(a) Isometric view

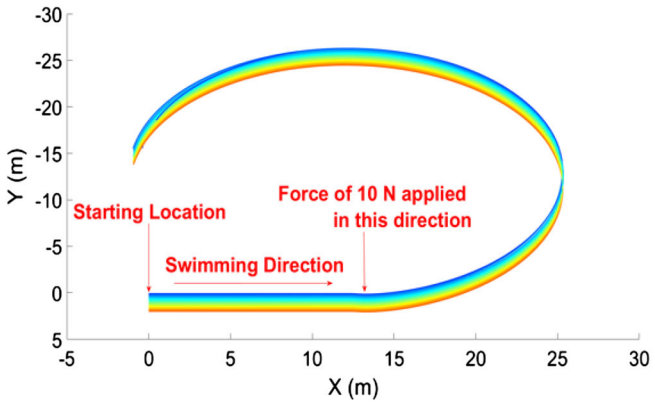

(b) Top view

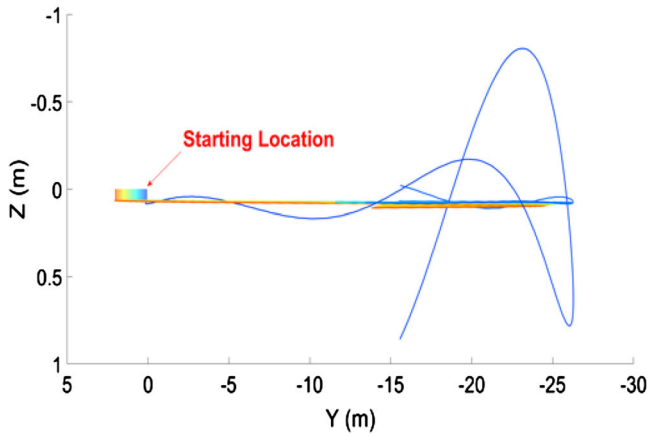

(c) Side view

Fig. 4 Simulated paths of a dorso-ventral flapping swimmer at different metacentric heights. Simulated path of the dorso-ventral flapping vehicle with a force of 10 N applied for 1 s after 36 s of forward swimming. 'z_g' (shown as 'zg' in Fig.) in these plots represent the metacentric height. **a–c** Shows path of the AUV in isometric, top and front views, respectively

generated from the cross-flow term 'M_{uw}'. The case presented here is for a specific body of an AUV. An analytical derivation for a more general case is presented in "Appendix B".

For a single case of Dorso-ventral flapping with sideways disturbance the variations in Roll, Pitch and Yaw orientations of the vehicle have been shown in the Fig. 5a. The simulated Surge forces and the Yaw moment acting on

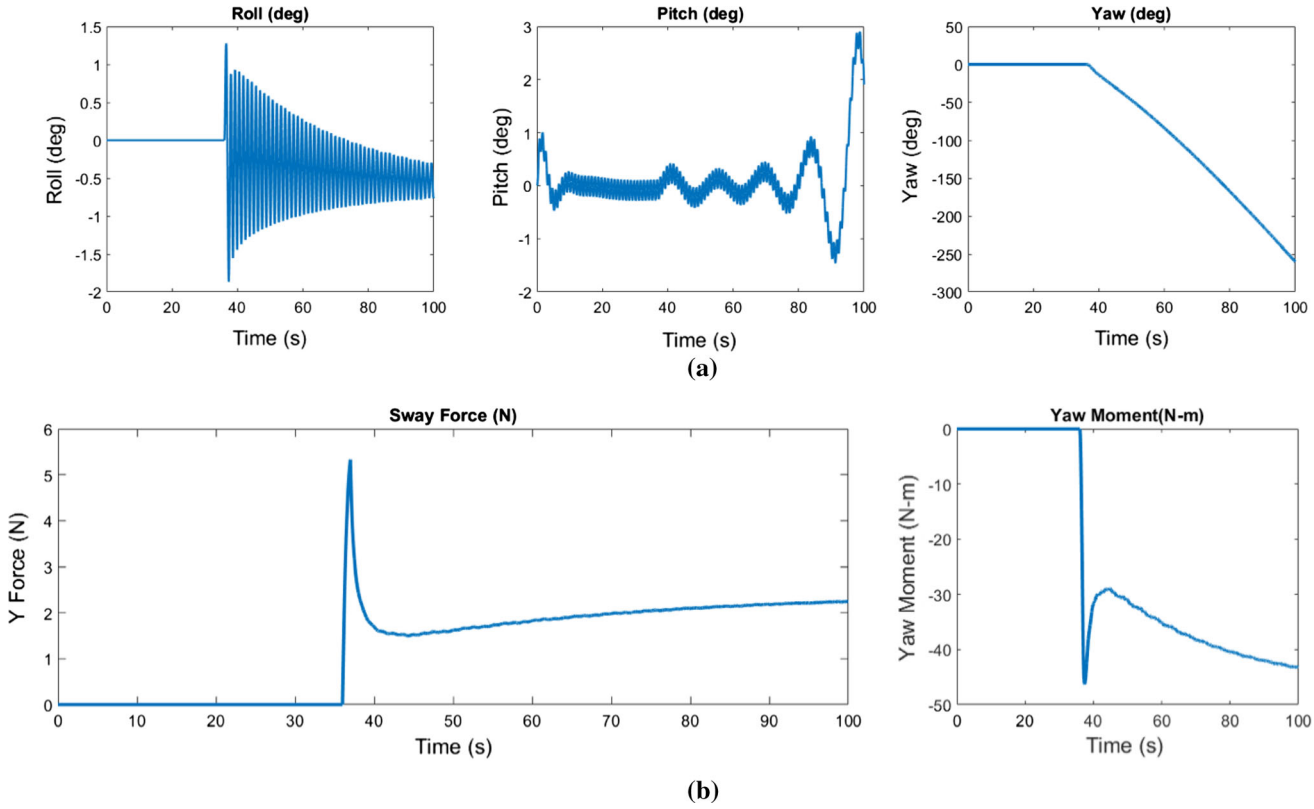

Fig. 5 Simulated orientations and forces acting on the swimmer. **a** Simulated roll, pitch and yaw angles of the swimmer along the path. **b** Simulated surge force and yaw moments acting on the swimmer along the path

the vehicle during the time of flight have been plotted in Fig. 5b. The peak rise in the Sway force (Fig. 5b), between 20 and 40 s is because of the simulated disturbance which causes the vehicle to spiral. This disturbance pushes the vehicle in the sway direction leading also to a spike in the yaw moment as described earlier. The oscillation in the pitch and roll plots are due to the offset in the propulsion and disturbance forces relative to the center of gravity of the vehicle.

Controllability of rotational oscillations

The wake from body oscillations could affect the propulsive performance of the caudal fin (Xiong and Lauder 2014). Xiong and Lauder (2014) and Lauder (2015a, b), for example, claim that an improvement in thrust performance is possible with effective control of body or head oscillations. As our study is restricted to thunniform swimming modes, body instead of head-oscillation, is considered (since the head does not have much relative motion with the body in this mode). Ideally, one could control body oscillation amplitudes by controlling the projected area of the body. For sideways flapping cases, this would be the projected area in the sagittal plane and in the frontal plane for dorso-ventral flapping. Another approach, as discussed here, would be to adjust the value of metacentric height in dorso-ventral flapping vehicles to get the required body oscillation amplitude. With sideways flapping, this would not be possible and adjusting the body's projected area in the sagittal plane would be the only option. Therefore, if the body oscillation amplitude is to be controlled without adjusting its projected area, dorso-ventral flapping should be preferred. Results from the numerical simulation highlighting this claim are presented here.

The relation between metacentric height, frequency and amplitude of pitching motion is illustrated in Fig. 6. It can be observed that, in general, the amplitude of pitching motion is reduced at higher frequencies of caudal oscillation. Also, low values of metacentric height lead to high amplitudes at low frequencies. We note that the value of the resonance frequency also depends on the value of the metacentric height as this value determines the stiffness in the pitching axis. This is also the reason for increased amplitude at particular frequencies for higher values of metacentric height. It can be seen that this peak in amplitude shifts towards the left for lower values of metacentric height. This is consistent with the fact that the resonance frequency decreases with decreasing pitching stiffness of the system (where stiffness in this case is directly proportional to the metacentric height of the vehicle).

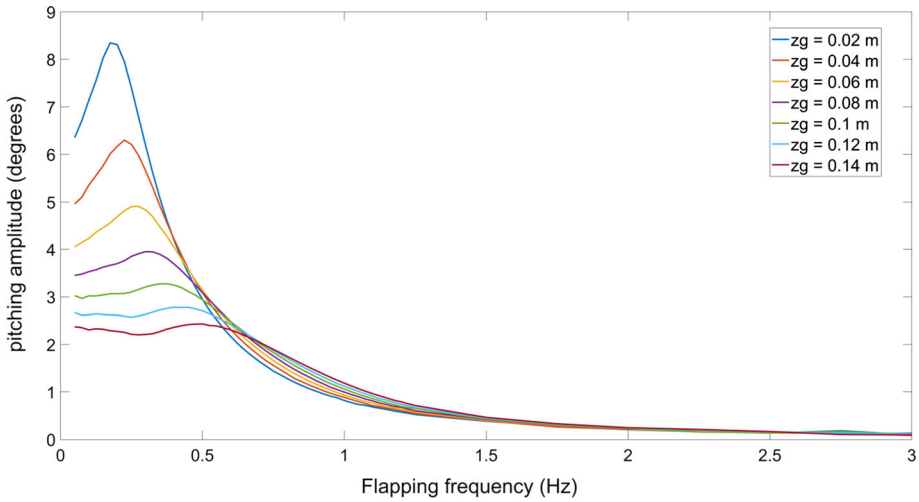

Fig. 6 Relation between flapping frequency and pitching amplitude for dorso-ventral flapping. Plot showing relation between metacentric height (z_g—shown as 'zg' in the Fig), flapping frequency and body oscillation amplitude in the pitch axis simulated using the parameters of REMUS underwater vehicle (Goldberg 1988)

Center of mass oscillations

The effect of center of mass oscillations on the energetics of swimming vehicles makes it worthwhile studying, for insight in the context of the choice of flapping orientation. In the previous subsection, it was shown that dorso-ventral flapping allows for better controllability of pitch oscillations. Here, the center of mass oscillations are indirectly measured from the total distance travelled by the swimmer. This gives a measure of the distance travelled by the swimmer for the same propulsive thrust for the same amount of time. High center of mass oscillation amplitudes will lead to shorter travel distance and vice versa. This travel length is calculated for various values of metacentric height and shown in Fig. 7.

It is observed that swimmers with sideways flapping travelled shorter distances than swimmers with dorso-ventral flapping (see Fig. 7). However, this is perhaps because of a circular path taken by sideways flapping swimmers under self-propelled and uncontrolled conditions (see Fig. 2). However, even when a rudder control input was given to correct the vehicle to maintain a straight-line path, taking care to ensure that the rudder inputs were realistic, the distance travelled was found to be typically lesser than that achieved by dorso-ventral flapping cases. Only an aggressive controller was able to extend the distance travelled to almost that of dorso-ventral flapping cases, but such a controller may be difficult to implement in practice. Also, such an aggressive control of the propellers would also lead to increased power consumption. The nearly constant value of distances travelled after a certain value of metacentric height in Fig. 7 is because of the dominance of restoring torques at high metacentric heights. The lower values of distances at low metacentric heights are primarily because of the heave oscillations, which are very low at high metacentric heights (see Fig. 4).

COM oscillation is not the sole factor that would influence the travel distance of the swimmer. This is evident from the results shown in Fig. 2, where one could see the differences between the path for sideways flapping and dorso-ventral flapping with disturbance, for the same conditions. Sideways flapping has a wavy path with more amplitude (see Fig. 2c) than that of the dorso-ventral flapping and attains a shorter travel distance, but a slightly different path (clearly visible in Fig. 2b), which is because of the differences in the axis of propulsive forces between the two flapping orientations. This slightly different path (as viewed from the top) can also influence the travel distance. Nevertheless, as seen in those images, the difference in path is very less compared to the deviations in the COM oscillation (see Fig. 2b and c). This persuades us

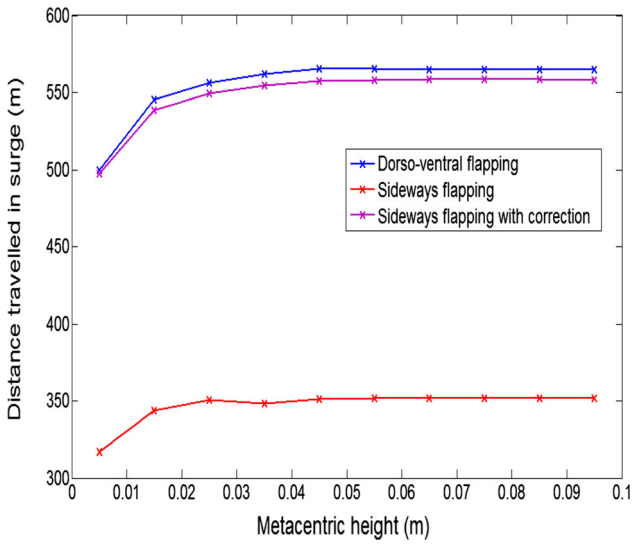

Fig. 7 Simulated distance travelled for different flapping orientations. Plot comparing the distance travelled by swimmers in surge with different orientations of flapping axis and different metacentric heights

to a conclusion that the COM oscillation is more dominant in influencing the travel distance.

Discussion

The aim of this study is to find the effects of choice of the flapping axis orientation on the swimming performance. Numerical simulations using validated models from literature suggest that dorso-ventral flapping allows for better stability in the absence of a control system, yields lesser Centre of Mass (COM) oscillation amplitude (also, in the absence of a robust control system) and also allows control in body rotational oscillations.

Dorso-ventral flapping swimmers were shown to realize a straight-line path as expected in the absence of a disturbing force, while sideways flapping yields a circular path in the absence of a control input. As most control systems rely on sensory information, a self-stable system would be more reliable even in the case of a sensor failure. For instance, in the event of an inertial measurement unit (IMU) (Webb and Weihs 2015) failure, a vehicle with sideways flapping would suffer in even maintaining a straight-line path. This is more important considering that many of the IMUs are unreliable or inaccurate in the yaw axis (Webb 2005) in the presence of electromagnetic interferences.

It was seen that dorso-ventral flapping offers controllability of rotational oscillations to favour propulsive performance of the vehicle (Lauder 2015; Xiong and Lauder 2014). It is also reported that dolphins and other aquatic animals may benefit in terms of propulsive performance from their head swing motion (Lauder 2015). However, very few studies in literature exist about the effect of body oscillations on the propulsive performance. Body oscillation control is also important in the case of observation class vehicles where a stable visual feed from an on-board camera is crucial. Dorso-ventral flapping with a careful choice of flapping frequency and metacentric height could minimise body oscillations for a high-quality visual feed.

It was shown that dorso-ventral flapping swimmers travelled more distance than sideways flapping cases for the same propulsive thrust, showing that the former could be more efficient. However, with a controller in place, the difference in the distance travelled is small. This small difference is primarily because of the sway motion in the sideways flapping swimmers which cannot be avoided. We must note here, that the power consumed for actuating the control surfaces for this correction is not considered. Nevertheless, our studies show overall, dorso-ventral swimming would be more efficient (albeit slightly sometimes) in all cases. The difference could be more pronounced in other cases of body's dynamic parameters or may be negligible in cases of bodies with minimal pitch oscillations. We note that the body underwent pitching oscillations in both cases of flapping axes because of the location of the propulsive force application on the body.

In our studies, the propulsive forces were applied on the center of buoyancy instead of the center of gravity, which initiated pitch oscillations that were amplified because of cross-flow interactions. If the propulsive force was directly applied on the center of gravity, the pitching oscillations could have been avoided. However, in practice propulsive forces can rarely be along the center of gravity. In general, sideways flapping axis cases would have a three-dimensional COM motion (surge, sway and heave) (Christ and Wernli 2007) whereas dorso-ventral flapping cases would have it only along two dimensions (surge and heave). It is also interesting to know the effects of an inclined flapping axis generating forces in surge sway and heave similar to the case of a heterocercal caudal fin (SNAME 1964). Further analysis in this aspect is limited in view of the scope of this article which is primarily to expose differences in performance with different flapping orientations. Nevertheless, this research could open avenues of development through a focus on the analysis of the relationship between center of mass oscillations and flapping axis orientation on different vehicle models.

The results from the analysis in this article can help robotic engineers in developing caudal fin propelled underwater robots. Recent advances in underwater actuators, especially with more compact ionic polymers (Prestero 2001) and soft actuators (Swarrup et al. 2019; Katzschmann et al. 2018) has led to the development of advanced robotic systems for underwater inspections and surveillance. This demands more understanding of the swimming dynamics of such robots to design efficient systems. The study in this article would help the engineers to decide the flapping orientation depending on their overall objectives. On the other hand, bio-inspired pectoral fin-propelled underwater robots are also popular. However, it is known that the fastest speeds are achieved with the caudal fin actuated swimming modes (Katzschmann et al. 2018) and that the pectoral fin-based swimming modes are good for manoeuvrability, and in addition, undulatory swimming of eels have also been known to have a low cost of transport (Chu et al. 2012). In view of these aspects, it is the choice of the engineer to choose the swimming modes depending on the end use.

Conclusions

A numerical study on the effects of flapping axis orientation was conducted on thunniform swimming mode, which allowed the idealization to consider an AUV body for the

analysis. A self-stable dorso-ventral flapping was found to advantageous in many cases, especially in terms of body-oscillation control and energetics. Results leading to this conclusion were presented individually in categories of stability, rotational oscillation and center of mass motions. Limitations of the study and future directions were also discussed in view of the unavailability of existing literature on this topic; for instance, the effect of pressure with respect to depth and assumption of thrust forces to be sinusoidal are a few limitations. Nonetheless, we hope that this study would open avenues of research towards this new area which is totally unexplored.

Appendix A

See Tables 1 and 2.

Table 1 Values of parameters and non-linear coefficients of REMUS underwater vehicle

Parameters	Value	Units	Description
W	299	N	Weight of the vehicle
B	299	N	Buoyancy of the vehicle
X_{prop}	3.86	N	X-direction thrust due to flapping foil
Y_{prop}	1.93	N	Y-direction force due to flapping foil
Z_{prop}	1.93	N	Z- direction force due to flapping foil
K_{prop}	0	N-m	Roll moment due to flapping foil
M_{prop}	0.115	N-m	Pitch moment due to flapping foil
N_{prop}	0.115	N-m	Yaw moment due to flapping foil
$X_{u\|u\|}$	− 1.62e+000	kg/m	Cross-flow Drag
$X_{\dot{u}}$	− 9.30e−001	kg	Added Mass
X_{wq}	− 3.55e+001	kg/rad	Added Mass Cross-term
$X_{q\|q\|}$	− 1.93e+000	kg-m/rad^2	Added Mass Cross-term
X_{vr}	+ 3.55e+001	kg/rad	Added Mass Cross-term
$X_{r\|r\|}$	− 1.93e+000	kg-m/rad^2	Added Mass Cross-term
$Y_{v\|v\|}$	− 1.31e+003	kg/m	Cross-flow Drag
$Y_{r\|r\|}$	+ 6. 32e−001	kg-m/rad^2	Cross-flow Drag
Y_{uv}	− 2.86e+001	kg/m	Body Lift Force and Fin Lift
$Y_{\dot{v}}$	− 3.55e+001	kg	Added Mass
$Y_{\dot{r}}$	+ 1.93e+000	kg-m/rad	Added Mass
Y_{ur}	+ 5.22e+000	kg/rad	Added Mass Cross Term and Fin Lift
Y_{wp}	+ 3.55e+001	kg/rad	Added Mass Cross-term
Y_{pq}	+ 1.93e+000	kg-m/rad^2	Added Mass Cross-term
$Z_{w\|w\|}$	− 1.31e+002	kg/m	Cross-flow Drag
$Z_{q\|q\|}$	+ 6.32e−001	kg-m/rad^2	Cross-flow Drag
Z_{wu}	− 2.86e+001	kg/m	Body Lift Force and Fin Lift
$Z_{\dot{w}}$	− 3.55e+001	kg	Added Mass
$Z_{\dot{q}}$	− 1.93e+000	kg-m/rad	Added Mass
Z_{up}	− 5.22e+000	kg/rad	Added Mass Cross-term and Fin Lift
Z_{vp}	− 3.55e+001	kg/rad	Added Mass Cross-term
Z_{rp}	+ 1.93e+000	kg-m/rad^2	Added Mass Cross-term
$K_{p\|p\|}$	− 1.30e−001	kg-m^2/rad ^{2}	Rolling Resistance
$K_{\dot{p}}$	- 7.04e−002	kg-m^2/rad	Added Mass
$M_{w\|w\|}$	+ 3.18e+000	kg	Cross-flow Drag
$M_{q\|q\|}$	− 1.88e+002	kg-m^2/rad^2	Cross-flow Drag
M_{uw}	+ 2.40e+001	kg	Body and Fin Lift and Munk Moment
$M_{\dot{w}}$	− 1.93e+000	kg-m	Added Mass
$M_{\dot{q}}$	− 4.88e+000	kg-m^2/rad	Added Mass
M_{uq}	− 2.00e + 000	kg-m/rad	Added Mass Cross Term and Fin Lift
M_{vp}	− 1.93e + 000	kg-m/rad	Added Mass Cross Term
M_{rp}	+ 4.86e+000	kg-m^2/rad^2	Added Mass Cross-term

Table 1 (continued)

Parameters	Value	Units	Description
$N_{v\|v\|}$	− 3.18e+000	kg	Cross-flow Drag
$N_{r\|r\|}$	− 9.40e+001	kg-m^2/rad^2	Cross-flow Drag
N_{uv}	− 2.40e+001	kg	Body and Fin Lift and Munk Moment
$N_{\dot{v}}$	+ 1.93e+000	kg-m	Added Mass
$N_{\dot{r}}$	− 4.88e+000	kg-m^2/rad	Added Mass
N_{ur}	− 2.00e+000	kg-m/rad	Added Mass Cross Term and Fin Lift
N_{wp}	− 1.93e+000	kg-m/rad	Added Mass Cross Term
N_{qp}	− 4.86e+000	kg-m^2/rad^2	Added Mass Cross-term
x_g	+ 0.0e+000	m	Centre of gravity (x-co-ordinate)
y_g	+ 0.0e+000	m	Centre of gravity (y-co-ordinate)
z_g	+ 1.96e-002	m	Centre of gravity (z-co-ordinate)
x_b	+ 0.0e+000	m	Centre of buoyancy (x-co-ordinate)
y_b	+ 0.0e+000	m	Centre of buoyancy (y-co-ordinate)
z_b	+ 0.0e+000	m	Centre of buoyancy (z-co-ordinate)

X, Y, Z, K, M and *N* represent values in surge, sway, heave, roll, pitch and yaw axes, respectively

Table 2 Descriptions of all the symbols used in the equations

Symbol	Units	Description
η	–	Displacement vector
η_1	–	Linear displacement vector
η_2	–	Angular displacement vector
x	m	x-position
y	m	y-position
z	m	z-position
ϕ	rad	Angular orientation with roll
θ	rad	Angular displacement in yaw
ψ	rad	Angular displacement in pitch
v	–	Velocity vector
$\dot{x}$	m/sec	Velocity in x-direction
$\dot{y}$	m/sec	Velocity in y-direction
$\dot{z}$	m/sec	Velocity in z-direction
$\dot{\phi}$	rad/sec	Angular velocity roll
$\dot{\theta}$	rad/sec	Angular velocity yaw
$\dot{\psi}$	rad/sec	Angular velocity pitch
X	N	Force along x-direction
Y	N	Force along y-direction
Z	N	Force along z-direction
K	N-m	Moment about x-direction
M	N-m	Moment about y-direction
N	N-m	Moment about z-direction

Appendix B

Stability for a generalised case

The study conducted in the article for stability in sideways flapping and dorso-ventral flapping is for a specific set of body shape parameters. For the sake of completeness, a generalised case is also presented here for obtaining the relation between stability and body hydrodynamic coefficients of underwater robots. This analytical derivation is adapted Edward V. Lewis 1989 (Lauder 2015).

Consider a swimmer following a straight-line motion confined to a single plane (e.g., considering forces acting only in the x and y plane—see Fig. 1). The forces X (surge), Y (sway) and N (yaw) in different directions equations can be written as:

$$Y = F_Y(u, v, \dot{u}, \dot{v}, r, \dot{r}) \tag{14a}$$

$$N = F_N(u, v, \dot{u}, \dot{v}, r, \dot{r}) \tag{14b}$$

where u is the velocity in the x-direction, v is the velocity in the y-direction, $\dot{u}$ is the acceleration in the x-direction, $\dot{v}$ is the acceleration in the y direction, r is the angular velocity about yaw axis, $\dot{r}$ is the angular acceleration about the yaw axis.

For obtaining the expression defining the dynamic stability of the system, the above equations are reduced to useful mathematical expressions using Taylor series expansions about a given initial equilibrium point u_1, v_1, $\dot{u}_1$,$\dot{v}_1$,r_1, $\dot{r}_1$ as shown below:

$$X = F_X(u_1, v_1, \dot{u}_1, \dot{v}_1, r_1, \dot{r}_1) + (u - u_1)\frac{\delta X}{\delta u} + (v - v_1)\frac{\delta X}{\delta v} + \ldots + (\dot{r} - \dot{r}_1)\frac{\delta X}{\delta \dot{r}} \tag{15a}$$

$$Y = F_Y(u_1, v_1, \dot{u}_1, \dot{v}_1, r_1, \dot{r}_1) + (u - u_1)\frac{\delta Y}{\delta u} + (v - v_1)\frac{\delta Y}{\delta v} + \ldots + (\dot{r} - \dot{r}_1)\frac{\delta Y}{\delta \dot{r}} \tag{15b}$$

$$N = F_n(u_1, v_1, \dot{u}_1, \dot{v}_1, r_1, \dot{r}_1) + (u - u_1)\frac{\delta N}{\delta u} + (v - v_1)\frac{\delta N}{\delta v} + \ldots + (\dot{r} - \dot{r}_1)\frac{\delta N}{\delta \dot{r}} \tag{15c}$$

For a body moving with a uniform velocity, initially $\dot{u}_1$, $\dot{v}_1$, r_1, $\dot{r}_1$, vanish because there is no acceleration while at equilibrium when moving with constant speed. Moreover, since most AUV's are symmetric about the x–z plane, the cross-flow terms $\partial y/\partial u = \partial y/\partial \dot{u} = 0$

Therefore, a change in forward velocity or acceleration does not produce any transverse force on the swimmer, and hence this term is neglected. Since we are assuming that the swimmer moves with uniform velocity in x-direction, there can be no transverse force acting on the swimmer at the initial state i.e., $F_y(u_1, v_1, \dot{u}_1, \dot{v}_1, r_1, \dot{r}_1)$=0. Thus, equation (15a, 15b, 15c) can be reduced to,

$$Y = \left(\frac{\partial Y}{\partial v}\right)v + \left(\frac{\partial Y}{\partial \dot{v}}\right)\dot{v} + \left(\frac{\partial Y}{\partial r}\right)r + \left(\frac{\partial Y}{\partial \dot{r}}\right)\dot{r} \tag{16a}$$

Similarly, the yawing moment can be written as:

$$N = \left(\frac{\partial N}{\partial v}\right)v + \left(\frac{\partial N}{\partial \dot{v}}\right)\dot{v} + \left(\frac{\partial N}{\partial r}\right)r + \left(\frac{\partial N}{\partial \dot{r}}\right)\dot{r} \tag{16b}$$

Since we are considering the effect of transverse disturbance, the relevant terms are only the sway force and yaw moment. Hence, the effect on surge force is not discussed here. The equations obtained here are for the forces with respect to the axis fixed on the vehicle; hence their effect on the acceleration is given below:

$$X = M(\dot{u} - vr) \tag{17a}$$

$$Y = M(\dot{v} + ur) \tag{17b}$$

$$N = I_Z\dot{r} \tag{17c}$$

Substituting (16a) and (16b) in (17a) and (17b) and simplifying, we get the following equations,

$$-\left(\frac{\partial Y}{\partial v}\right)v + \left(M - \frac{\partial Y}{\partial \dot{v}}\right)\dot{v} - \left(\frac{\partial Y}{\partial r} - Mu_1\right)r - \left(\frac{\partial Y}{\partial \dot{r}}\right)\dot{r} = 0 \tag{18a}$$

$$-\left(\frac{\partial N}{\partial v}\right)v - \left(\frac{\partial N}{\partial \dot{v}}\right)\dot{v} - \left(\frac{\partial N}{\partial r}\right)r + \left(I_Z - \left(\frac{\partial N}{\partial \dot{r}}\right)\right)\dot{r} = 0 \tag{18b}$$

In Eq. (18a), all the terms have units of force and in Eq. (18b) all the terms have units of the moment. Non-dimensionalizing by dividing the first equation with $(\rho/2)L^2V^2$ and second equation with $(\rho/2)L^3V^2$ and using primed symbols for non-dimensionalized terms this yields:

$$-Y_{v\prime}v\prime + (M\prime - Y_{\dot{v}})\dot{v}\prime - (Y_{r\prime} - M\prime)r\prime - Y_{\dot{r}\prime}\dot{r}\prime = 0 \tag{19a}$$

$$-N_{v\prime}v\prime - N_{\dot{v}}\dot{v}\prime - N_{r\prime}r\prime + \left(I'_z - N_{\dot{r}\prime}\right)\dot{r}\prime = 0 \tag{19b}$$

where,

$$M\prime = \frac{M}{\rho\frac{L^3}{2}}; v\prime = \frac{v}{V}; \dot{v}\prime = \frac{\dot{v}L}{V^2}; I'_z = \frac{I_Z}{\rho\frac{L^2}{2}}; r\prime = \frac{rL}{V}; \dot{r}\prime = \frac{\dot{r}L^2}{V^2}$$

$$Y_{v\prime} = \frac{Y_v}{\left(\frac{\rho}{2}\right)L^2V}; Y_{r\prime} = \frac{Y_r}{\left(\frac{\rho}{2}\right)L^3V}; N_{v\prime} = \frac{N_v}{\left(\frac{\rho}{2}\right)L^3V}; N_{r\prime} = \frac{N_r}{\left(\frac{\rho}{2}\right)L^4V}$$

$$Y_{\dot{v}\prime} = \frac{Y_{\dot{v}}}{\left(\frac{\rho}{2}\right)L^3}; Y_{\dot{r}\prime} = \frac{Y_{\dot{r}}}{\left(\frac{\rho}{2}\right)L^4}; N_{\dot{v}\prime} = \frac{N_{\dot{v}}}{\left(\frac{\rho}{2}\right)L^4}; N_{\dot{r}\prime} = \frac{N_{\dot{r}}}{\left(\frac{\rho}{2}\right)L^5}$$

(Y_v represents $\partial Y/\partial v$, N_v represents $\partial N/\partial v$ and so on).

Using only these linear terms, solutions to yaw and sway terms can be obtained to analyse the swimmer's stability. Equations B.6(a) and B.6(b) are two simultaneous differential equations of the first order in two unknowns—the transverse velocity component v' and the yaw angular velocity component r'. The standard solutions of the first-order equation are as follows:

$$v\prime = V_1e^{\sigma_1 t} + V_2e^{\sigma_2 t} \tag{20a}$$

$$r\prime = R_1e^{\sigma_1 t} + R_2e^{\sigma_2 t} \tag{20b}$$

where new parameters V_1, V_2, R_1 and R_2 are constants of integration; σ_1 and σ_2 are known as stability indices.

In the above equation, if both σ_1 and σ_2 are negative, both v' and r' will approach zero with the passage of time. In this case, the swimmer would reach a straight-line motion without yawing or drifting in the transverse direction. However, if both of them are positive, v' and r' will increase continuously over time leaving the swimmer spiralling and never returns back to its original course. The stability of the vehicle also depends on the magnitude of these indices. If they have high magnitude and are both negative then the vehicle is more stable and will reach the straight-line motion more rapidly.

These indices can be found out by substituting equations B.7(a) and B.7(b) in equation B.6, and simplification gives a quadratic equation in σ as shown below:

$$A\sigma^2 + B\sigma + C = 0 \tag{21}$$

where

$$A = \left(I'_z - N_{\dot{r}\prime}\right)M\prime\dot{v}\prime; B = -\left(I'_z - N_{\dot{r}\prime}\right)Y_{v\prime} - M\prime N_{r\prime};$$

$$C = Y_{v\prime}N_{r\prime} - (Yr\prime - M\prime)N_{v\prime}$$

By finding out these values of A, B and C we can obtain the stability indices as shown below:

$$\sigma_{1,2} = \frac{-B \pm \sqrt{B^2 - 4AC}}{2A} \tag{22}$$

References

Christ RD, Wernli R (2007) The ROV manual, 2nd edn. Butterworth-Heinemann, Massachusetts

Chu Won-Shik et al (2012) Review of biomimetic underwater robots using smart actuators. Int J Precis Eng Manuf 13(7):1281–1292

Cook M (2012) Flight dynamics principles: a linear systems approach to aircraft stability and control 3rd Edition, Massachusetts. Butterworth-Heinemann, USA

Fish F (2004) Structure and mechanics of nonpiscine control surfaces. IEEE J Ocean Eng 29:605–621

Fish F (2016) Secondary evolution of aquatic propulsion in higher vertebrates: validation and prospect. Integr Comp Biol 56:1285–1297

Goldberg L (1988) Principles of naval architecture. I: stability and strength. The Society of Naval Architects and Marine Engineers, New York

Jimenez A, Seco F, Prieto J, Guevara J (2010) Indoor pedestrian navigation using an INS/EKF framework for yaw drift reduction and a foot-mounted IMU. In: 2010 7th workshop on positioning, navigation and communication, Dresden, Germany

Katzschmann RK, DelPreto J, MacCurdy R, Rus D (2018) Exploration of underwater life with an acoustically controlled soft robotic fish. Sci Robot 3(16):eaar3449

Krishnadas A, Ravichandran S, Rajagopal P (2018) Analysis of biomimetic caudal fin shapes for optimal propulsive efficiency. Ocean Eng J 153:132–142

Lauder G (2000) Function of the caudal fin during locomotion in fishes: kinematics, flow visualization, and evolutionary patterns. Am Zool 40:101–122

Lauder G (2015a) Fish locomotion: recent advances and new directions. Ann Rev Mar Sci 7:521–545

Lauder GV (2015b) Fish locomotion: recent advances and new directions. Annu Rev Mar Sci 7(1):521–545

Lauder G, Drucker E (2002) Forces, fishes, and fluids: hydrodynamic mechanisms of aquatic locomotion. News Physiol Sci 17:235–240

Lewis EV (1989) Principles of naval architecture second revision, volume (III), motion in waves and controllability. The Society of Naval Architects and Marine Engineers, Jersey City

Li N et al (2017) Numerical study on the hydrodynamics of thunniform bio-inspired swimming under self-propulsion. PLoS One 12:e0174740

Liu et al. (2016) Fin-body interaction and its hydrodynamic benefits in fish's steady swimming. In: APS Meeting Abstracts, Baltimore, Maryland

"MATLAB R2014a", The MathWorks Inc. (2014) [Online]. https://www.mathworks.com/. Accessed 27 July 2017

Morrison M (1987) Inertial measurement unit. USA Patent US4711125A, 8 December

Prestero T (2001) Verification of a six-degree of freedom simulation model for the remus autonomous underwater vehicle. M.S. Thesis, Department of Mechanical Engineering at Massachusetts Institute of Technology and Woods Hole Oceanographic Institute, Massachusetts, USA

SNAME (1964) Nomenclature for treating the motion of a submerged body through a fluid. Society of Naval Architects and Marine Engineers, New York

Swarrup S, Ganguli R, Madras G (2019) Studies to improve the actuation capability of low-frequency IPMC actuator for underwater robotic applications. ISSS J Micro Smart Syst 8:41–47

Webb PW (2005) Stability and maneuverability. Fish Physiol 23:281–332

Webb P, Weihs D (2015) Stability versus maneuvering: challenges for stability during swimming by fishes. Integr Comp Biol 55:753–764

Xia DC et al (2016) Effect of head swing motion on hydrodynamic performance of fishlike robot propulsion. J Hydrodyn 28:637–647

Xiong G, Lauder G (2014) Center of mass motion in swimming fish: effects of speed and locomotor mode during undulatory propulsion. Zoology 117:269–281